Production of selected cosmogenic radionuclides by muons: 2. Capture of negative muons

B. Heisinger [a], D. Lal [b], A.J.T. Jull [c], P. Kubik [d], S. Ivy-Ochs [d], K. Knie [a], E. Nolte [a,*]

[a] *Faculty of Physics, Technical University of Munich, D-85747 Garching, Germany*
[b] *Scripps Institution of Oceanography, UCSD, La Jolla, CA 92093, USA*
[c] *University of Arizona, NSF Arizona AMS Laboratory, Tucson, AZ 85721, USA*
[d] *Paul Scherrer Institute, c/o ETH-Hönggerberg, CH-8093 Zurich, Switzerland*

Abstract

We have determined the production yields for radionuclides in Al_2O_3, SiO_2, S, Ar, K_2SO_4, $CaCO_3$, Fe, Ni and Cu targets, which were irradiated with slow negative muons at the Paul Scherrer Institute in Villigen (Switzerland). The fluences of the stopped negative muons were determined by measuring the muonic X-rays. The concentrations of the long-lived and short-lived radionuclides were measured with accelerator mass spectrometry (AMS) and γ-spectroscopy, respectively. Special emphasis was put on the radionuclides ^{10}Be, ^{14}C and ^{26}Al produced in quartz targets, ^{26}Al in Al_2O_3 and S targets, ^{36}Cl in K_2SO_4 and $CaCO_3$ targets, and ^{53}Mn in Fe_2O_3 targets. These targets were selected because they are also the naturally occurring target minerals for cosmic ray interactions in typical rocks. We also present results of calculations for depth-dependent production rates of radionuclides produced after cosmic ray μ⁻ capture, as well as cosmic ray-induced production rates of geologically relevant radionuclides produced by the nucleonic component, by μ⁻ capture, by fast muons and by neutron capture. © 2002 Elsevier Science B.V. All rights reserved.

Keywords: cosmogenic elements; radio-active isotopes; production; rates

1. Introduction

At depths between about 10 and 100 hg/cm² below the Earth's surface, the dominant production mode in the lithosphere for many radionuclides is cosmic ray negative muon capture. At shallow depths up to about 10 hg/cm², production of radionuclides by the nucleonic component of the cosmic rays is dominant (see e.g. [1–3]). At greater depths, typically below about 100 hg/cm², the dominant production mode is due to fast muon-induced reactions. The background production of radionuclides is due to neutrons originating from spontaneous fission of ^{238}U and from α decays of ^{235,238}U and ^{232}Th [4]. To unravel the irradiation history of a rock exposed at near and below sea-level depths, one has to there-

* Corresponding author. Tel.: +49-89-289-12554;
Fax: +49-89-289-14280.
E-mail address: nolte@physik.tu-muenchen.de (E. Nolte).

fore explicitly take into account the cosmogenic production of nuclides due to capture of stopping negative muons. The μ^- capture by a nucleus is followed by the emission of a few particles, on average by about one nucleon for light target nuclei [5]. The yield of radionuclides from a particular nucleus depends on the particle emission probabilities.

In this paper we present the results of our studies of yields of radionuclides from several targets. For completeness, we also summarize here the results of our earlier studies of yields of ^{10}Be, ^{26}Al and ^{36}Cl in μ^- capture [6–8]. Calculations of depth-dependent production rates of radionuclides by cosmic ray μ^- capture are given. Using the present results we also give for some geologically important radionuclides and minerals surface and depth-integrated production rates due to the nucleonic component, to stopped μ^-, and to fast muons of the cosmic radiation and to neutron capture.

Our results of studies of production of several radionuclides in similar targets exposed to fast muons of 100 GeV and 190 GeV energies are reported in [9].
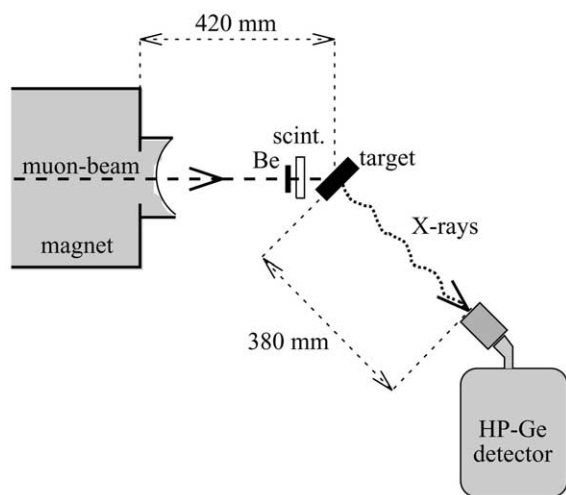

Fig. 1. Experimental setup for irradiations of targets with slow negative muons at the μE4 channel at PSI Villigen (Switzerland).

2. Irradiations with slow negative muons

The targets Al_2O_3, SiO_2, S, Ar, K_2SO_4, $CaCO_3$, Fe, Ni and Cu were irradiated with slow negative muons at the μE4 beam line of the Paul Scherrer Institute (PSI) in Villigen, Switzerland, to measure particle emission channels leading to the production of radionuclides after μ^- capture. The experimental setup is shown in Fig. 1. The muonic X-rays were measured in-beam with a coaxial high-purity germanium detector (Hp-Ge) to determine the fluence of stopped negative muons in the targets. This detector was also used to measure in-beam the groundstate γ transitions in the residual nuclei produced after μ^- capture and particle emission. Details are described in [10].

3. Experimental procedures

The short-lived radionuclides with half-lives longer than typically 1 day were measured off-line without any physical or chemical processing at the Technical University of Munich using a lead-shielded, low-background setup with a coaxial Hp-Ge detector identical to the one used at PSI.

For the determination of ^{10}Be and ^{26}Al in quartz, the targets were physically and chemically processed according to procedures described in [7,11]. The concentrations of these two radionuclides were measured using the AMS facilities at ETH Hönggerberg [12], and at the Munich accelerator laboratory [7], respectively. Separate SiO_2 targets were used for AMS measurements of ^{14}C. The wet extraction of ^{14}C from those targets was performed at the Scripps Institution of Oceanography, La Jolla, CA, USA, and the AMS measurements of ^{14}C were performed at the University of Arizona NSF Facility, Tucson, AZ, USA [13].

For the determination of ^{36}Cl in the K_2SO_4 target, NaCl carrier was added and the target was dissolved in HNO_3. A stochiometric quantity of $BaNO_3$ was added to precipitate sulfur as $BaSO_4$. After filtration, a small quantity of $BaNO_3$ was added again. The solution was filtered, $AgNO_3$ was added and AgCl precipitate

was obtained. The $CaCO_3$ target was processed as described in [10] to obtain an AgCl sample. The [36]Cl measurement was performed with post-accelerated completely stripped Cl ions at the Munich accelerator laboratory [14]. The Fe targets were processed as described in [9] and [53]Mn was measured using the gas-filled magnet at the Munich accelerator laboratory [15].

4. Experimental results

In Table 1 we present the results of measured effective probabilities $f^*({}^A Z)$ for production of the nuclide ${}^A Z$ after μ^- capture in the target nucleus in the respective target elements, together with the previously reported values of the Munich group [6–8] and of other groups [16–19]. The effective probabilities for each element are calculated from the measured rate of negative muon capture in the element, which is based on measurements of the muonic X-rays, and from the yield of the radionuclide measured by AMS, off-line γ-spectroscopy or in-beam γ-spectroscopy of the groundstate γ transitions in the final nuclei produced after μ^- capture and particle emission. Note that in the case of in-beam γ-spectroscopy of the ground state γ transitions, the radionuclide yields are only lower limits. For the radionuclide production from the elements, O and Si, the target used was SiO_2; for K it was K_2SO_4 and for calcium $CaCO_3$.

For those effective production probabilities f^* relevant to earth sciences applications, we have combined present and earlier results of investigations of the Munich group into weighted means. The measured f^* of $0.41 \pm 0.03\%$ for [10]Be from O compares well with the value of $0.49 \pm 0.06\%$ published earlier [6]. Combining these results, we obtain a mean value of $f^* = 0.43 \pm 0.03\%$. In the case of [26]Al from Si, the measured value of $2.1 \pm 0.2\%$ is in excellent agreement with the earlier values of $1.9 \pm 0.6\%$ [6] and $2.4 \pm 0.3\%$ [7]. Combining these three results, we obtain a mean value of $f^* = 2.2 \pm 0.2\%$. A mean value of $f^* = 0.17 \pm 0.02\%$ is derived for the yield of [26]Al from S using the present value of $0.19 \pm 0.03\%$ and the previous

value of $0.14 \pm 0.03\%$ [6]. Similarly, for [36]Cl from Ca, we obtain a mean value of $f^* = 4.5 \pm 0.5\%$ using the present value of $4.3 \pm 0.5\%$ and the previous value of $6.1 \pm 2.0\%$ [8]. This yield agrees perfectly well with $f^* = 4.3 \pm 0.8\%$ determined in a geologic measurement in calcite [19].

The two [53]Mn determinations in the present study, $10.0 \pm 1.5\%$ and $8.3 \pm 1.0\%$ give a mean value of $f^* = 8.9 \pm 0.8\%$ for [53]Mn from Fe. Finally, for [39]Cl and [38]Cl from Ar, the yields are determined to be $f^* = 41.7 \pm 4.0\%$ and $f^* = 7.9 \pm 1.0\%$, respectively.

5. Production of radionuclides by negative muon capture

5.1. Stopping rate of negative muons

The rate $R_{\mu^-}(h)$ of stopped negative muons in the lithosphere as function of depth h is obtained by differentiating the total negative muon flux:

$$\Phi_{\mu^-}(h) = f_{\mu^-}(h) \cdot \Phi(h) \qquad (1)$$

$\Phi(h)$ is the total flux of positive and negative muons related to the vertical muon flux $\Phi_v(h)$ by the relation:

$$\Phi(h) = \int_{2\pi} \Phi(h, \theta) \cdot d\Omega = \int_{2\pi} \Phi_v(h) \cdot \cos^{n(h)} \Theta \cdot d\Omega =$$

$$\frac{2\pi}{\Theta n(h) + 1} \cdot \Phi_v(h) \qquad (2)$$

For lithospheric depths $h < 2000$ hg/cm² $\Phi_v(h)$ is given by [20–24]:

$$\Phi_v(h) = \frac{258.5}{(h + 210) \cdot ([h + 10]^{1.66} + 75)} \cdot$$

$$e^{-5.5 \cdot 10^{-4} \cdot h} \text{ cm}^{-2} \text{ s}^{-1} \text{ sr}^{-1} \qquad h < 2000 \text{ hg/cm}^2 \qquad (3)$$

The fraction of negative muons is:

Table 1
Target elements, produced radionuclides, half-lives $T_{1/2}$, main reactions, detection methods and particle emission channel probabilities f^* to these radionuclides (present and previous work)

Target element	Nuclide	$T_{1/2}$	Main reaction	Method	f^* (%)
O	^{7}Be	53.3 days	^{16}O$(\mu^-,\nu_\mu\alpha p4n)$	off-line γ	0.02 ± 0.01
O	^{10}Be	1.6 Ma	^{16}O$(\mu^-,\nu_\mu\alpha pn)$	AMS	0.41 ± 0.03
					0.49 ± 0.06 [6]
					0.43 ± 0.03^a
O	^{14}C	5730 a	^{16}O$(\mu^-,\nu_\mu pn)$	AMS	13.7 ± 1.1
Al	^{22}Na	2.6 a	^{27}Al$(\mu^-,\nu_\mu p4n)$	off-line γ	0.05 ± 0.01
Al	^{24}Na	15.0 h	^{27}Al$(\mu^-,\nu_\mu p2n)$	off-line γ	2.1 ± 0.2
					3.5 ± 0.8 [16]
Al	^{25}Na+	59.6 s	^{27}Al$(\mu^-,\nu_\mu pn)+$		
	^{25}Mg	stable	^{27}Al$(\mu^-,\nu_\mu 2n)$	in-beam γ	> 6.4
Al	^{26}Na+	1.07 s	^{27}Al$(\mu^-,\nu_\mu p)+$		
	^{26}Mg	stable	^{27}Al$(\mu^-,\nu_\mu n)$	in-beam γ	> 37.7
Al	^{27}Mg	9.46 min	^{27}Al(μ^-,ν_μ)	off-line γ	12.0 ± 0.7
Si	^{22}Na	2.6 a	^{28}Si$(\mu^-,\nu_\mu p4n)$	off-line γ	0.15 ± 0.03
Si	^{24}Na	15.0 h	^{28}Si$(\mu^-,\nu_\mu p2n)$	off-line γ	3.4 ± 0.2
Si	^{26}Na+	1.07 s	^{28}Si$(\mu^-,\nu_\mu 2p)+$		
	^{26}Mg	stable	^{28}Si$(\mu^-,\nu_\mu pn)$	in-beam γ	> 5.4
				in-beam γ	> 9.0 [17]
Si	^{27}Mg+	9.46 min	^{28}Si$(\mu^-,\nu_\mu p)+$		
	^{27}Al	stable	^{28}Si$(\mu^-,\nu_\mu n)$	in-beam γ	> 23.8
				in-beam γ	> 25.8 [17]
Si	^{26}Al	716 ka	^{28}Si$(\mu^-,\nu_\mu 2n)$	AMS	2.1 ± 0.2
				AMS	2.4 ± 0.3 [7]
				AMS	1.9 ± 0.6 [6]
				AMS	2.2 ± 0.2^a
Si	^{28}Al	2.25 min	^{28}Si(μ^-,ν_μ)	in-beam γ	22.8 ± 2.5
				in-beam γ	26 ± 3 [17]
S	^{26}Al	716 ka	^{32}S$(\mu^-,\nu_\mu\alpha 2n)$	AMS	0.19 ± 0.03
				AMS	0.14 ± 0.02 [6]
				AMS	0.17 ± 0.02^a
Ar	^{38}Cl	37.2 min	^{40}Ar$(\mu^-,\nu_\mu 2n)$	off-line γ	7.9 ± 1.0
Ar	^{39}S+	11.5 s	^{40}Ar$(\mu^-,\nu_\mu p)+$		
	^{39}Cl	56 min	^{40}Ar$(\mu^-,\nu_\mu n)$	off-line γ	41.7 ± 4.0
K	^{36}Cl	301 ka	^{39}K$(\mu^-,\nu_\mu p2n)$	AMS	3.5 ± 0.5
Ca	^{36}Cl	301 ka	^{40}Ca$(\mu^-,\nu_\mu\alpha)$	AMS	4.3 ± 0.5
				AMS	6.1 ± 2.0 [8]
				AMS	4.5 ± 0.5^a
				AMS	3.0 ± 1.0 [17]
				AMS	4.3 ± 0.8 [18]
Fe	^{47}Sc	3.35 days	^{56}Fe$(\mu^-,\nu_\mu 2\alpha n)$	off-line γ	0.0025 ± 0.0005
Fe	^{48}Sc	43.7 h	^{56}Fe$(\mu^-,\nu_\mu 2\alpha)$	off-line γ	0.007 ± 0.002
Fe	^{48}V	16.0 days	^{54}Fe$(\mu^-,\nu_\mu\alpha 2n)$	off-line γ	0.04 ± 0.01
Fe	^{52}V+	3.75 min	^{56}Fe$(\mu^-,\nu_\mu\alpha)+$		
	^{52}Cr	stable	^{56}Fe$(\mu^-,\nu_\mu p3n)$	in-beam γ	> 2.05
Fe	^{51}Cr+	27.7 days	^{54}Fe$(\mu^-,\nu_\mu p2n)+$		
	^{51}Mn	46.2 min	^{54}Fe$(\mu^-,\nu_\mu 3n)$	off-line γ	0.62 ± 0.05
Fe	^{53}Cr	stable	^{56}Fe$(\mu^-,\nu_\mu p2n)$	in-beam γ	> 1.33
Fe	^{54}Cr	stable	^{56}Fe$(\mu^-,\nu_\mu pn)$	in-beam γ	> 3.0
Fe	^{55}Cr	3.5 min	^{56}Fe$(\mu^-,\nu_\mu p)$	in-beam γ	> 1.66
Fe	^{52}Mn	5.6 days	^{56}Fe$(\mu^-,\nu_\mu 4n)$	off-line γ	0.19 ± 0.02
				off-line γ	$0,22 \pm 0.2$ [16]

Table 1 (*Continued*).

Target element	Nuclide	$T_{1/2}$	Main reaction	Method	f* (%)
Fe	$^{52}Mn^m$	21 months	$^{56}Fe(\mu^-,\nu_\mu 4n)$	off-line γ	0.50 ± 0.10
Fe	^{53}Mn	3.7 Ma	$^{56}Fe(\mu^-,\nu_\mu 3n)$	AMS	10.0 ± 1.5
					8.3 ± 1.0
					8.9 ± 0.8[a]
Fe	^{54}Mn	312 days	$^{56}Fe(\mu^-,\nu_\mu 2n)$	off-line γ	18.7 ± 1.1
				off-line γ	21.2 ± 1.5 [16]
Fe	^{55}Mn	stable	$^{56}Fe(\mu^-,\nu_\mu n)$	in-beam γ	> 34.2
Fe	^{56}Mn	2.58 h	$^{56}Fe(\mu^-,\nu_\mu)$	off-line γ	17.4 ± 1.0
				off-line γ	20.1 ± 1.3 [16]
Ni	^{48}V	16.0 days	$^{58}Ni(\mu^-,\nu_\mu 2\alpha 2n)$	off-line γ	0.012 ± 0.003
Ni	^{51}Cr	27.7 days	$^{58}Ni(\mu^-,\nu_\mu \alpha p2n)$	off-line γ	0.19 ± 0.05
Ni	^{52}Mn	5.6 days	$^{58}Ni(\mu^-,\nu_\mu \alpha 2n)$	off-line γ	0.094 ± 0.009
				off-line γ	0.12 ± 0.01 [16]
Ni	^{54}Mn	312 days	$^{58}Ni(\mu^-,\nu_\mu \alpha)$	off-line γ	1.38 ± 0.05
				off-line γ	1.9 ± 0.2 [16]
Ni	^{56}Mn	2.58 h	$^{60}Ni(\mu^-,\nu_\mu \alpha)$	off-line γ	0.25 ± 0.03
Ni	$^{57}Mn+$	1.5 months	$^{60}Ni(\mu^-,\nu_\mu 2pn)+$		
	^{57}Fe	stable	$^{60}Ni(\mu^-,\nu_\mu p2n)$	in-beam γ	> 1.48
Ni	$^{58}Mn+$	3 s	$^{62}Ni(\mu^-,\alpha)+$		
	^{58}Fe	stable	$^{60}Ni(\mu^-,\nu_\mu pn)$	in-beam γ	> 1.3
Ni	$^{53}Fe+$	8.51 months	$^{58}Ni(\mu^-,\nu_\mu p4n)+$		
	^{53}Co	0.24 s	$^{58}Ni(\mu^-,\nu_\mu 5n)$	off-line γ	0.04 ± 0.02
Ni	$^{54}Fe+$	stable	$^{58}Ni(\mu^-,\nu_\mu p3n)+$		
	^{54}Co	0.193 s	$^{58}Ni(\mu^-,\nu_\mu 4n)$	in-beam γ	> 0.64
Ni	^{55}Fe	2.73 a	$^{58}Ni(\mu^-,\nu_\mu p2n)$	in-beam γ	> 1.22
Ni	^{56}Fe	stable	$^{58}Ni(\mu^-,\nu_\mu pn)$	in-beam γ	> 10.5
Ni	^{59}Fe	44.5 days	$^{60}Ni(\mu^-,\nu_\mu p)$	off-line γ	0.41 ± 0.02
				off-line γ	0.56 ± 0.06
Ni	$^{61}Fe+$	6.0 months	$^{62}Ni(\mu^-,\nu_\mu p)+$		
	^{61}Co	1.65 h	$^{62}Ni(\mu^-,\nu_\mu n)$	off-line γ	1.75 ± 0.10
				off-line γ	2.9 ± 0.5 [16]
Ni	^{55}Co	17.5 h	$^{58}Ni(\mu^-,\nu_\mu 3n)$	off-line γ	0.25 ± 0.08
				off-line γ	0.36 ± 0.11 [16]
Ni	^{56}Co	77.3 days	$^{58}Ni(\mu^-,\nu_\mu 2n)$	off-line γ	3.57 ± 0.06
				off-line γ	4.6 ± 0.5 [16]
Ni	^{57}Co	272 days	$^{58}Ni(\mu^-,\nu_\mu n)$	off-line γ	32.1 ± 1.5
				off-line γ	41.3 ± 2.9 [16]
Ni	^{58}Co	70.9 days	$^{58}Ni(\mu^-,\nu_\mu)$	off-line γ	17.1 ± 0.6
Ni	^{59}Co	stable	$^{60}Ni(\mu^-,\nu_\mu n)$	in-beam γ	> 9.2
Ni	^{60}Co	5.27 a	$^{60}Ni(\mu^-,\nu_\mu)$	off-line γ	6.82 ± 0.11
				off-line γ	7.9 ± 0.6 [16]
Ni	$^{62}Co^m$	14.0 months	$^{62}Ni(\mu^-,\nu_\mu)$	off-line γ	0.053 ± 0.008
Cu	^{54}Mn	312 days	$^{63}Cu(\mu^-,\nu_\mu \alpha p4n)$	off-line γ	0.010 ± 0.004
Cu	^{56}Mn	2.58 h	$^{63}Cu(\mu^-,\nu_\mu \alpha p2n)$	off-line γ	0.045 ± 0.005
Cu	^{58}Fe	stable	$^{63}Cu(\mu^-,\nu_\mu \alpha n)$	in-beam γ	> 0.72
Cu	^{59}Fe	44.5 days	$^{63}Cu(\mu^-,\nu_\mu \alpha)$	off-line γ	0.27 ± 0.01
Cu	$^{61}Fe+$	6.0 months	$^{63}Cu(\mu^-,\nu_\mu 2p)+$		
	^{61}Co	1.65 h	$^{63}Cu(\mu^-,\nu_\mu pn)$	off-line γ	1.25 ± 0.05
Cu	^{57}Co	272 days	$^{63}Cu(\mu^-,\nu_\mu p5n)$	off-line γ	0.030 ± 0.003
Cu	^{58}Co	70.9 days	$^{63}Cu(\mu^-,\nu_\mu p4n)$	off-line γ	0.21 ± 0.1
Cu	^{60}Co	5.27 a	$^{63}Cu(\mu^-,\nu_\mu p2n)$	off-line γ	0.96 ± 0.04
Cu	$^{62}Co+$	1.5 months	$^{63}Cu(\mu^-,\nu_\mu p)+$		
	^{62}Ni	stable	$^{63}Cu(\mu^-,\nu_\mu n)$	in-beam γ	> 35.5

Table 1 (*Continued*).

Target element	Nuclide	$T_{1/2}$	Main reaction	Method	f^* (%)
Cu	$^{62}Co^m$	14.0 months	$^{63}Cu(\mu^-,\nu_\mu p)$	off-line γ	0.16 ± 0.01
Cu	$^{63}Co+$	27.5 s	$^{65}Cu(\mu^-,\nu_\mu pn)+$		
	^{63}Ni	100 a	$^{63}Cu(\mu^-,\nu_\mu)$	in-beam γ	> 6.97
Cu	$^{64}Co+$	0.3 s	$^{65}Cu(\mu^-,\nu_\mu p)+$		
	^{64}Ni	stable	$^{65}Cu(\mu^-,\nu_\mu n)$	in-beam γ	> 12.2
Cu	^{57}Ni	36.0 h	$^{63}Cu(\mu^-,\nu_\mu 6n)$	off-line γ	0.008 ± 0.002
Cu	^{58}Ni	stable	$^{63}Cu(\mu^-,\nu_\mu 5n)$	in-beam γ	> 0.9
Cu	^{60}Ni	stable	$^{63}Cu(\mu^-,\nu_\mu 3n)$	in-beam γ	> 3.2
Cu	^{61}Ni	stable	$^{63}Cu(\mu^-,\nu_\mu 2n)$	in-beam γ	> 8.2
Cu	^{65}Ni	2.52 h	$^{65}Cu(\mu^-,\nu_\mu)$	off-line γ	1.91 ± 0.0

f^* is obtained from Eq. 11.
[a] Mean value of experiments performed by the Munich group.

$$f_{\mu^-}(h) = \frac{1}{K_\mu + 1} \qquad (4)$$

where K_μ is the ratio of positive to negative muons. A compilation of K_μ values is shown in Fig. 2 [25–28]. A recent systematic investigation of K_μ for muon energies higher than 10 GeV using average values of nine energy groups [25] yields a mean value of $K_\mu = 1.268 \pm (0.008 + 0.002 \cdot E[\text{GeV}])$. Fig. 2 shows that K_μ can be considered constant at 1.268 for energies $E > 4$ GeV. For lower energies, K_μ seems to decrease with decreasing energy. There is evidence that the effect is stronger for higher geomagnetic cut-off rigidity R_C. Such an effect could be expected from the ratio of primary to secondary cosmic ray particles [29]. It would influence the stopping rate of negative muons. Since, however, the mean muon energies are around 10 GeV, where stopped negative muon-induced production becomes dominant, the
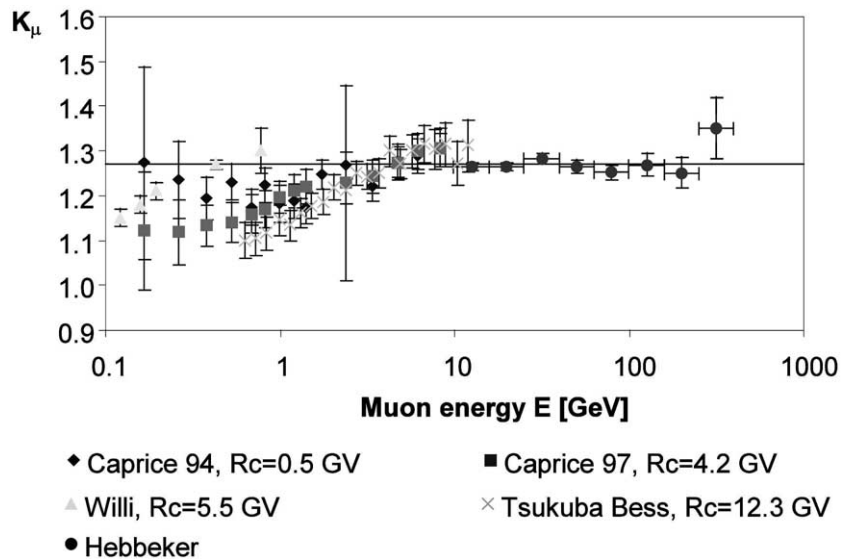

Fig. 2. Ratio K_μ of positive to negative muons as function of muon energy. Mean values of nine energy groups above 10 GeV [25], CAPRICE 94 [26] with a geomagnetic cut-off rigidity $R_C = 0.5$ GV, CAPRICE 97 [26] with $R_C = 4.2$ GV, WILLI [27] with $R_C = 5.6$ GV, Tsukuba BESS with [28] $R_C = 11.5$ GV.

effect is considered to be small. With $K_\mu = 1.268$, $f_{\mu^-}(h) = 1/(1 + 1.268) = 0.44$ is obtained.

The exponent $n(h)$ can be expressed by [9]:

$$n(h) = 3.21 - 0.297 \cdot \ln(h + 42) + 1.21 \cdot 10^{-3} \cdot h \qquad (5)$$

The rate of stopped negative muons can then be calculated from Eqs. 1–5:

$$R_{\mu^-}(h) = \frac{\mathrm{d}}{\mathrm{d}h}\left(\Phi_v(h) \cdot \frac{2\pi}{n(h)+1} \cdot f_{\mu^-}\right) \approx$$

$$f_{\mu^-} \cdot \frac{\mathrm{d}}{\mathrm{d}h}\left(\Phi_v(h) \cdot \frac{2\pi}{n(h)+1}\right) \qquad (6)$$

$R_{\mu^-}(h)$ as function of lithospheric depth is shown in Fig. 3 together with experimental data [30–32]. At sea level, the rate of stopped negative muons is obtained to be:

$$R_{\mu^-}(0) = 190 \text{ g}^{-1} \text{ a}^{-1}. \qquad (7)$$

Our rate $R_{\mu^-}(h)$ agrees well with values given in [33], while the stopping rate for shallow depths as given in [19] is lower by about 20%.

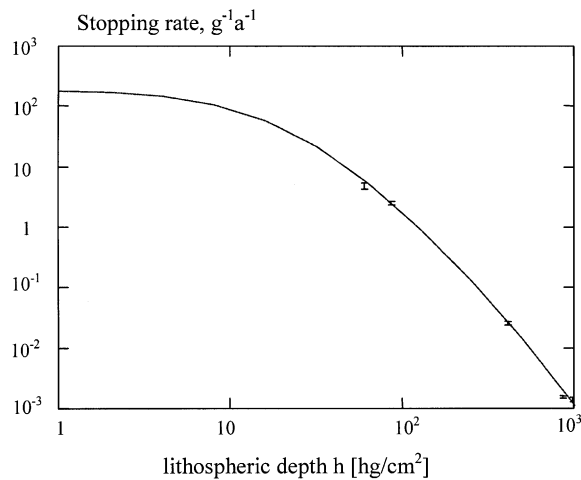The depth-integrated rate $\Phi_{\mu^-}(0)$ of stopped negative muons can be written as:

Fig. 3. Rate of stopped negative muons $R_{\mu^-}(h)$ as function of lithospheric depth h together with the experimental values of [30–32].

$$\Phi_{\mu^-}(0) = \Phi(0) \cdot f_{\mu^-}(0) =$$

$$\int_0^\infty R_{\mu^-}(h) \cdot \mathrm{d}h = R_{\mu^-}(0) \cdot \Lambda_{\mu^-} \qquad (8)$$

Λ_{μ^-} is the absorption mean free path for stopped negative muons:

$$\Lambda_{\mu^-} = 15.1 \text{ hg/cm}^2 \qquad (9)$$

It can be used to obtain approximate estimates of the rate of stopped negative muons:

$$R_{\mu^-}(h) \approx R_{\mu^-}(0) \cdot e^{-\frac{h}{\Lambda_{\mu^-}}} \qquad (10)$$

5.2. Production rate of radionuclides in the capture of negative muons

The production rate $P_{\mu^-}(h)$ of the radionuclide ^AZ from the target element Z_t in a specific chemical compound due to negative muon capture is given by:

$$P_{\mu^-}(h) = R_{\mu^-}(h) \cdot f_C(Z_t) \cdot f_D(Z_t) \cdot f^*(^AZ) \qquad (11)$$

where $f_C(Z_t)$ is the chemical compound factor [34], $f_D(Z_t)$ is the probability that the negative muon does not decay in the K-shell before nuclear capture [35], and $f^*(^AZ)$ is the effective probability for production of the nuclide ^AZ after μ^- capture in the target nucleus. The integrated production rate in a column of unit cross-section is given by:

$$Q_{\mu^-} = P_{\mu^-}(0) \Lambda_{\mu^-} \qquad (12)$$

with $\Lambda_{\mu^-} = 15.1$ hg/cm^2. For comparison, the absorption mean free path for the production of nuclides by the nucleonic component of the cosmic rays is $\Lambda_h = 1.5$ hg/cm^2 [36].

6. Summary of production rates of radionuclides by the nucleonic component, by μ^- capture and by fast muons of the cosmic radiation

The measurements of this work allow the cal-

Table 2
Target compound, target, radionuclide produced, production rates $P_h(0)$, $P_{\mu^-}(0)$, $P_{\mu_f}(0)$, $\Sigma P(0)$ at sea level and high geomagnetic latitudes, depth-integrated production rates Q_h, Q_{μ^-}, Q_{μ_f}, ΣQ due to the hadronic component of the cosmic radiation (h), to μ^- capture (μ^-), to fast muons (μ_f) and to the sum of these contributions (Σ), chemical compound factor f_C [34], probability f_D that the muon does not decay [35], probability f^* for particle emission to the radionuclide, σ_0 fast muon-induced cross-section at 1 GeV

Compound	Target	Nuclide	$P_h(0)$ g^{-1} a^{-1}	Q_h m^{-2} a^{-1} ($\times 10^7$)	f_C	f_D	f^* %	$P_{\mu^-}(0)$ g^{-1} a^{-1}	Q_{μ^-} m^{-2} a^{-1} ($\times 10^7$)	σ_0 μb	$P_{\mu_f}(0)$ g^{-1} a^{-1}	Q_{μ_f} m^{-2} a^{-1} ($\times 10^7$)	$\Sigma P(0)$ g^{-1} a^{-1}	ΣQ m^{-2} a^{-1} ($\times 10^7$)
SiO_2	O	^{10}Be	5.31[a,b]	0.79	0.704	0.1828	0.43 ±0.03	0.106 ±0.007	0.16 ±0.01	1.84 ±0.25	0.093 ±0.013	0.41 ±0.06	5.51	1.4
SiO_2	O	^{14}C	18.4[c,d]	2.8	0.704	0.1828	13.7 ±1.1	3.34 ±0.27	5.0 ±0.4	8.8 ±4.9	0.44 ±0.25	1.9 ±1.1	21.3	9.8
SiO_2	Si	^{26}Al	31.8[a]	4.8	0.296	0.6559	2.2 ±0.2	0.805 ±0.073	1.2 ±0.1	27.6 ±3.3	0.715 ±0.086	3.1 ±0.4	33.3	9.1
H_2O	O	^{10}Be	8.86[a,b]	1.3	1	0.1828	0.43 ±0.03	0.15 ±0.01	0.23 ±0.02	1.84 ±0.25	0.155 ±0.021	0.68 ±0.09	9.16	2.2
H_2O	O	^{14}C	30.7[c,d]	4.6	1	0.1828	13.7 ±1.1	4.75 ±0.38	7.2 ±0.6	8.8 ±4.9	0.74 ±0.41	3.2 ±1.8	36.2	15
S	S	^{26}Al	10.2[e]	1.5	1	0.7475	0.17 ±0.02	0.241 ±0.028	0.36 ±0.40	4.3 ±1.2	0.203 ±0.055	0.89 ±0.24	10.6	2.8
K_2O	K	^{36}Cl	145[f,g] ±10	22	0.755	0.8020	3.5 ±0.5	4.07 ±0.58	6.1 ±0.9		2.90[e]	13	152	40
$CaCO_3$	Ca	^{36}Cl	18.6[f,h] ±0.6	2.8	0.361	0.8486	4.5 ±0.5	2.59 ±0.29	3.9 ±0.4	27.4 ±5.9	0.296 ±0.063	1.3 ±0.3	21.5	8.0
Fe_2O_3	Fe	^{53}Mn	110[i,j]	17	0.682	0.9062	8.9 ±0.8	10.45 ±0.94	16.0 ±1	75 ±21	1.43 ±0.41	6.3 ±1.8	122	39

culation of the in situ production of radionuclides in the lithosphere due to capture of negative muons in various target elements. With the help of [9], fast muon-induced nuclide production rates can also be calculated. For completeness cosmic ray-induced productions by the nucleonic component, are also included here. In Table 2 the production rates $P_h(0)$, $P_{\mu^-}(0)$, $P_{\mu_f}(0)$ and the depth-integrated production rates Q_h, Q_{μ^-}, Q_{μ_f} of the long-lived cosmogenic radionuclides ^{10}Be, ^{14}C and ^{26}Al from quartz (SiO_2), of ^{10}Be and ^{14}C from ice (H_2O), of ^{26}Al from S and $CaCO_3$, of ^{36}Cl from K_2O and $CaCO_3$, and of ^{53}Mn from Fe_2O_3 are listed for sea level and high geomagnetic latitudes.

$P_h(0)$ and Q_h are the production rates due to the hadronic component of the cosmic radiation. For the calculations the hadronic productions of ^{10}Be in quartz and ice [37,38], of ^{14}C in quartz and ice [37] and of ^{26}Al in quartz [13,39] were used. These measurements of total production rates $\Sigma P_\lambda(h)$ were performed at non-vanishing altitude h and at the magnetic latitude λ. In [36], an atmospheric attenuation length for muons of $\Lambda_{\mu,a} = 2.47$ hg/cm^2 is given. For altitudes up to $y = 1000$ m, in [25] the altitude dependence is described by $e^{y/L}$ with $L = 4900$ m $+ 750$ m$\cdot p$[GeV/c]. For a mean momentum $p \approx 7$ GeV/c relevant for altitudes of a few km [9], $\Lambda_{\mu,a} = 12$ hg/cm^2 is calculated. In [45], the altitude dependence is given by $e^{-h/\Lambda_{\mu,a}}$ where the atmospheric altitude h in hg/cm^2 here has to be taken negative. Sea level corresponds to $h = 0$ For $0 < -h < 8.4$ hg/cm^2: $\Lambda_{\mu,a} = (2.63 \pm 0.14 + (1.50 \pm 0.15)p[\text{GeV/c}])$ hg/cm^2. For atmospheric muon momenta $p \approx 7$ GeV/c [9], $\Lambda_{\mu,a} = 13$ hg/cm^2 is obtained. The atmospheric stopping rate of negative muons is thus given by:

$$R_{\mu^-,a}(h) = \frac{\mathrm{d}}{\mathrm{d}h}\left(\Phi_v(0)\cdot e^{-h/\Lambda_{\mu,a}}\cdot\frac{2\pi}{n(h)+1}\cdot f_{\mu^-}\right)$$

(13)

From Eq. 13 the atmospheric attenuation length for stopping negative muons is calculated to be $\Lambda_{\mu^-,a} \approx 13.5$ hg/cm^2 which is by 10% smaller than the mean lithospheric length $\Lambda_{\mu^-} = 15.1$ hg/cm^2. $R_{\mu^-,a}(0) = 215$ g^{-1} a^{-1} is obtained. By taking the actual mean muon momentum at sea level $p \approx 7.7$ GeV/c [9], $R_{\mu^-,a}(0) = 197$ g^{-1} a^{-1} compares well with $R_{\mu^-}(0) = 190$ g^{-1} a^{-1}.

The production rates for negative muon capture $P_{\mu^-}(0)$ of the present paper were recalculated with Eq. 13 to the altitude of measurement and subtracted from the measured total production rates. The remaining contributions for hadronic and fast muon-induced production were recalculated to sea level and high magnetic latitudes $\lambda > 60°$ with the help of the latitude and altitude dependencies of nuclear disintegrations measured in the atmosphere [44]. These nuclear disintegrations with energy releases higher than 40 MeV are considered to include hadronic and fast muon-induced reactions but not μ^- capture reactions. In the case of ^{10}Be and ^{26}Al these present values differ slightly from those derived in [37,38]. For the hadronic production rates of ^{36}Cl in K_2O, of ^{36}Cl in $CaCO_3$ and of ^{53}Mn in Fe_2O_3 measurements and estimates reported in [40,41], [18,19,40] and [42,43], respectively, were used.

The uncertainties given for $P_{\mu^-}(0)$ and Q_{μ^-} are solely the standard deviations of f^*. Systematic errors introduced by f_C, f_D and $R_{\mu^-}(h)$ are not included in Table 2. These are considered to be $\leq 10\%$. The uncertainties given for $P_{\mu_f}(0)$ and Q_{μ_f} are the standard deviations of $\sigma(190$ GeV$)$. Uncertainties for α, the mean muon energy and the muon flux are not included in Table 2. If $\alpha = 0.75$ is increased by 10%, the cross-section $\sigma(35$ GeV$)$ calculated from $\sigma(190$ GeV$)$ is lower by 12%. This energy of 35 GeV is representative of the energy range where the fast muon production becomes dominant. Uncertainties in the muon energy and flux are considered to be in the range of 10% each.

Dependencies of the muon flux from the geomagnetic latitude can be found in [46]. The anisotropy reported in [46] is $\Phi^{90°}/\Phi^{0°} \approx 1.1$. Dependencies from the geomagnetic latitude are not considered here.

Fig. 4 shows the production rates of ^{10}Be, ^{14}C and ^{26}Al in quartz due to the nucleonic component, to μ^- capture and to fast muons and the sum of these contributions as function of depth at sea level and high latitudes. Production by muons becomes dominant below depths of about 10 hg/cm^2.
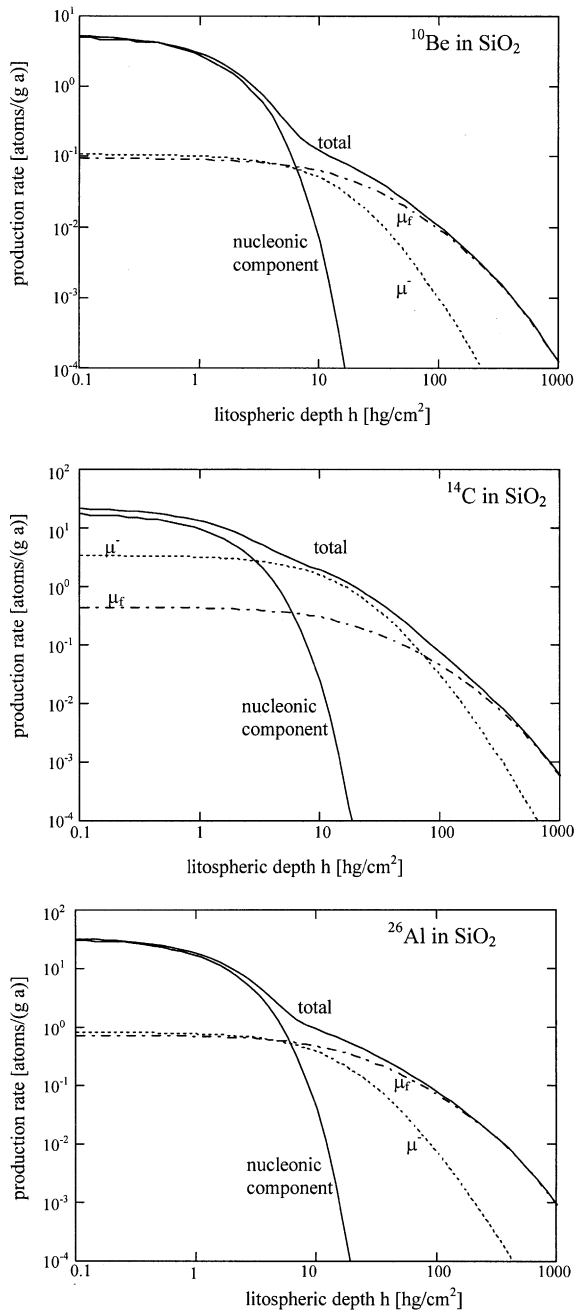
Fig. 4. Production rates of ^{10}Be, ^{14}C and ^{26}Al in quartz as function of lithospheric depth due to the hadronic component, to μ^- capture and to fast muons and total production rates, for sea level and high latitudes.

Due to parametrizations and calculations different from those of [3], the production rates presented here differ slightly for $P_{\mu^-}(0)$, but are a factor of 3.5 higher for $P_{\mu_f}(0)$. The depth-integrated production rates Q_{μ^-} and Q_{μ_f} agree reasonably well.

The ratio of production rates $P_{\mu^-,^{26}Al}/P_{\mu^-,^{10}Be} = 7.0 \pm 0.4$ measured by [47] agrees well with our surface production ratio of 7.6 ± 0.9. The ratios of $P_{^{26}Al}(13.28\ \mathrm{hg/cm^2})/P_{^{10}Be}(13.28\ \mathrm{hg/cm^2}) = 4.4 \pm 1.0$ and $P_{^{26}Al}(37.8\ \mathrm{hg/cm^2})/P_{^{10}Be}(37.8\ \mathrm{hg/cm^2}) = 3.7 \pm 1.5$ reported by [48], however, are measured in depths where fast muon-induced production is dominant (see Fig. 4). These ratios are significantly lower than our ratio of $P_{\mu_f,^{26}Al}/P_{\mu_f,^{10}Be} = 7.7 \pm 1.4$. Large differences in the production ratios for the nucleonic component and fast muons are not expected, if the fast muon-induced production is caused dominantly by hadronic showers (see Table 2). The ratio of the production rates due to the nucleonic component is $P_{h,^{26}Al}/P_{h,^{10}Be} = 6.0 \pm 0.5$ (see Table 2). Our fast muon ratio is thus in reasonable agreement with this value.

The relative μ^- contribution of 1–3% to the total ^{10}Be production rate at the surface measured by [49] is in good agreement with our value (see Table 2).

The atmospheric production rate of ^{39}Ar due to the decay of ^{39}Cl produced in the capture of negative muons by ^{40}Ar is calculated to be 0.13 atoms/m^2 s compared to 56 atoms/m^2 s due to nuclear reactions with ^{40}Ar [50].

7. Thermal neutron-induced production of radionuclides

For radionuclides as e.g. ^{36}Cl, ^{41}Ca, ^{59}Ni and ^{63}Ni the dominant reaction mechanism can be neutron capture. Neutrons in the lithosphere can be produced as secondary particles by the nucleonic component, by μ^- capture, by fast muons and by the decays of U and Th. $P_{n,h}$, P_{n,μ^-}, P_{n,μ_f} and $P_{n,U/Th}$ are the respective neutron production rates per mass unit and time. For the further discussion, the neutrons are considered thermalized at the depth h, where they are cap-

tured in the reaction $^{A-1}Z(n,\gamma)^A Z$. In the case of dominantly thermal neutron capture reactions, the fraction $f(^A Z)$ of neutrons producing the radionuclide $^A Z$ is given by:

$$f(^A Z) = \frac{a(^{A-1}Z)\cdot\sigma(^{A-1}Z(n_{\text{th}},\gamma)^A Z)}{\sum a(Z)\cdot\sigma_{\text{th}}(Z)} \qquad (14)$$

with the particle abundances $a(^{A-1}Z)$ and $a(Z)$ and the thermal neutron capture cross-sections $\sigma(^{A-1}Z(n_{\text{th}},\gamma)^A Z)$ and $\sigma_{\text{th}}(Z)$, respectively.

In the approximation that the decrease of the neutron flux $\Phi_{\text{h}}(0)\cdot e^{-h/\Lambda_{\text{h}}}$ is mainly due to scattering, the rate of thermalized neutrons at depth h is:

$$P_{\text{n,h}}(h) = \frac{\mathrm{d}\Phi_{\text{h}}(h)}{\mathrm{d}h} = \frac{\Phi_{\text{h}}(0)}{\Lambda_{\text{h}}}\cdot e^{-h/\Lambda_{\text{h}}} = 2525\frac{n}{g\cdot a}\cdot e^{-h/\Lambda_{\text{h}}} \qquad (15)$$

with $\Phi_{\text{h}}(0) = 0.012$ n/s cm^2 [51] at sea level and high latitudes. An albedo effect at the boundary atmosphere–lithosphere has not been taken into account. The production rate of the radionuclide would have to be normalized with an additional factor f_{norm}, which is of the order of 1.

The neutron production rate by μ^- capture is given by:

$$P_{\text{n,}\mu^-}(h) = \sum a(Z)\cdot f_{\text{C}}(Z)\cdot f_{\text{D}}(Z)\cdot f_{\text{n}}(Z)\cdot R_{\mu^-}(h) \qquad (16)$$

with the neutron yield $f_{\text{n}}(Z)$ after nuclear μ^- capture (see e.g. [5]). The chemical compound factors $f_{\text{C}}(Z)$ refer to the chemical composition of the mineral.

The fast muon-induced neutron production rate can be taken from [9]:

$$P_{\text{n,}\mu_{\text{f}}}(h) = 4.8\cdot 10^{-6}\ \text{g}^{-1}\ \text{cm}^2\ \beta(h)\cdot\Phi(h)\cdot\overline{E}^a \qquad (17)$$

The U/Th-induced neutron production rate $P_{\text{n,U/Th}}$ can be calculated using [4]. The production rate of the radionuclide $^A Z$ by neutron capture is then given by:

$$P_{\text{n}}(h) = \{P_{\text{n,h}}(h)\cdot f_{\text{norm}} + P_{\text{n,}\mu^-}(h) +$$
$$P_{\text{n,}\mu_{\text{f}}}(h) + P_{\text{n,U/Th}}\}\cdot f(^A Z) \qquad (18)$$

Other U/Th-induced background reactions as e.g. $^{23}\text{Na}(\alpha,n)^{26}\text{Al}$ can be taken into account using [4].

8. Geological applications

Geological applications are determinations of erosion, ablation or uplift rates and of surface exposure ages. The production rate of a radionuclide is the sum of four contributions, hadronic production, μ^- capture, fast muon-induced production and neutron capture:

$$P(h) = P_{\text{h}}(h) + P_{\mu^-}(h) + P_{\mu_{\text{f}}}(h) + P_{\text{n}}(h) \qquad (19)$$

For the determination of erosion rates, one can calculate the number of radionuclides per gram, $N(h)$, at depth h below a surface, which is eroding with a rate ε and over a time t:

$$N(h) = \int_0^t \mathrm{d}t'\cdot P(h + \varepsilon\cdot t')\cdot e^{-t'/\tau} \qquad (20)$$

with the τ being the life time of the radionuclide. The integral can be calculated with the production rate formulas and parameters given in this paper using standard mathematical programs. For rough estimates exponential depth dependences as described in these papers can be used. For high erosion rates, the muon-induced production of radionuclides is comparable to that of the nucleonic component, as can be seen from the depth-integrated production rates Q in Table 2.

For determinations of exposure ages, prior exposure due to muon-induced activation at the depth h has to be taken into account. Not taking this properly into account would result in an overestimate of the exposure age of the order of:

$$\delta t \approx \frac{P(h)}{P(0)}\cdot\tau \qquad (21)$$

9. Conclusions

The data presented here yield fairly accurate estimates of production rates for several radionuclides in the atmosphere and in the lithosphere due to capture of negative muons. These data constitute an important supplement to the nuclide production rate estimates due to energetic nucleons [13,18,19,37–43], those due to fast muon-induced nuclear reactions [9], and due to low-energy radiogenic neutrons from U and Th decay processes [4]. It is of importance to many geological applications of cosmogenic radionuclides, and to a variety of underground nuclear physics experiments such as solar neutrino detection or search for dark matter.

References

[1] D. Lal, Chem. Geol. (Isot. Geosci. Sect.) 66 (1987) 89–98.

[2] B. Heisinger, M. Niedermayer, F.J. Hartmann, G. Korschinek, E. Nolte, G. Morteani, S. Neumaier, C. Petitjean, P. Kubik, A. Synal, S. Ivy-Ochs, In-situ production of radionuclides at great depths, Nucl. Instrum. Methods B 123 (1997) 341–346.

[3] B. Heisinger, E. Nolte, Cosmogenic in situ production of radionuclides: Exposure ages and erosion rates, Nucl. Instrum. Methods B 172 (2000) 790–795.

[4] Y. Feige, B.G. Oltman, J. Kastner, Production rates of neutrons in soils due to natural radioactivity, J. Geophys. Res. 73 (1968) 3135–3142.

[5] P. Singer, Emission of particles following muon capture in intermediate and heavy nuclei, in: Springer Tracts in Modern Physics 71, Nuclear Physics, Springer, Berlin, 1974, pp. 39–87.

[6] M. Niedermayer, Determination of Depth Profiles of the Cosmogenic Radionuclides ^{26}Al and ^{10}Be in Quartz and Sulfur Minerals with AMS (in German), Diploma thesis, Technical University of Munich, Germany, 1995.

[7] E. Strack, B. Heisinger, B. Dockhorn, F.J. Hartmann, G. Korschinek, E. Nolte, G. Morteani, C. Petitjean, S. Neumaier, Determination of erosion rates with cosmogenic ^{26}Al, Nucl. Instrum. Methods B 92 (1994) 317–320.

[8] B. Dockhorn, S. Neumaier, F.J. Hartmann, C. Petitjean, H. Faestermann, G. Korschinek, H. Morinaga, E. Nolte, Determination of erosion rates with cosmic ray produced ^{36}Cl, Z. Phys. A 341 (1991) 117–119.

[9] B. Heisinger, D. Lal, A.J.T. Jull, P. Kubik, S. Ivy-Ochs, S. Neumaier, K. Knie, V. Lazarev, E. Nolte, Production of selected cosmogenic radionuclides by muons: 1 Fast muons, Earth Planet. Sci. Lett. (2002).

[10] B. Heisinger, Muon Induced Production of Radionuclides (in German), Dissertation Technical University of Munich, 1998.

[11] C.P. Kohl, K. Nishizumi, Chemical isolation of quartz for measurements of in-situ-produced cosmogenic radionuclides, Geochim. Cosmochim. Acta 56 (1992) 3583–3587.

[12] H.-A. Synal, G. Bonani, M. Döbeli, R.M. Ender, P. Gartenmann, P.W. Kubik, Ch. Schnabel, M. Suter, Status report of the PSI/ETH AMS facility, Nucl. Instrum. Methods B 123 (1997) 62–68.

[13] D. Lal, A.J.T. Jull, Studies of cosmogenic in situ ^{14}CO and ^{14}CO$_2$ produced in terrestrial and extraterrestrial samples: experimental procedures and applications, Nucl. Instrum. Methods B 92 (1994) 291–296.

[14] P. Kubik, G. Korschinek, E. Nolte, Accelerator mass spectrometry with completely stripped ^{36}Cl ions at the Munich Postaccelerator, Nucl. Instrum. Methods B 1 (1984) 51–59.

[15] K. Knie, T. Faestermann, G. Korschinek, AMS at the Munich gas-filled analyzing magnet system GAMS, Nucl. Instrum. Methods B 123 (1997) 128–131.

[16] G. Heusser, T. Kirsten, Radioisotope production rates by muon capture, Nucl. Phys. A 195 (1972) 369–378.

[17] H.G. Miller, M. Eckhouse, P. Martin, R.E. Welsh, Yields of gamma ray emission following capture of negative muons by ^{32}Si and ^{24}Mg, Phys. Rev. C 6 (1972) 487–493.

[18] J. Stone, G.L. Allan, L.K. Fifield, J.M. Evans, A.R. Chivas, Limestone erosion measurements with cosmogenic chlorine-36 in calcite – preliminary results from Australia, Nucl. Instrum. Methods B 92 (1994) 311–316.

[19] J.O.H. Stone, J.M. Evans, L.K. Fifield, G.L. Allan, R.G. Cresswell, Cosmogenic chlorine-36 production in calcite by muons, Geochim. Cosmochim. Acta 62 (1998) 433–454.

[20] A.I. Barbouti, B.C. Rastin, A study of the absolute intensity of muons at sea level and under various thicknesses of absorber, J. Phys. G 9 (1983) 1577–1595.

[21] S. Miyake, V.S. Narasimham, P.V. Ramana Murthy, Cosmic-ray intensity measurements deep underground at depths of 800–8400 m.w.e., Nuovo Cimento 32 (1964) 1505–1523.

[22] Ch. Berger et al., Experimental study of muon bundles observed in the Fréjus detector, Phys. Rev. D 40 (1989) 2163–2171.

[23] M. Aglietta et al., Neutrino-induced and atmospheric single-muon fluxes measured over five decades of intensity by

LVD at Gran Sasso laboratory, Astropart. Phys. 3 (1995) 311–320.

[24] M. Ambrosio et al., Vertical muon intensity measured with MACRO at the Gran Sasso laboratory, Phys. Rev. D 52 (1995) 3793–3802.

[25] T. Hebbeker, C. Timmermanns, A compilation of high energy atmospheric muon data at sea level, arXiv:hep-ph/0102042 v 15 Feb 2001, Astropart. Phys., to be published.

[26] J. Kremer et al., Measurements of ground-level muons at two geomagnetic latitudes, Phys. Rev. Lett. 83 (1999) 4241–4244.

[27] B. Vulpescu, J. Wentz, I.M. Brancus, H. Rebel, A.F. Badea, H. Bozdog, H.J. Mathes, M. Duma, The charge ratio of atmospheric muons below 1.0 GeV/c by measuring the lifetime of muonic atoms in aluminium, J. Phys. G 27 (2001) 977–991.

[28] M. Motoki et al., Precise measurement of atmospheric muon fluxes at sea level, in: Proc. ICRC, 2001, pp. 927–991.

[29] H. Bilokon, G. Cini Castagnoli, A. Castellina, B. D'Ettore Piazzoli, G. Mannocchi, E. Meroni, P. Picchi, S. Vernetto, Flux of the vertical negative muons stopping at depths 0.35–1000 hg/cm^2, J. Geophys. Res. 94 (1989) 145–152.

[30] J.C. Barton, M. Slade, The intensity of stopping pions at sea level and underground, in: Proc. 9th ICRC, London, 1965, p. 1006.

[31] P.N. Bhat, P.V. Ramana Murthy, Intensity measurements of low energy cosmic ray muons underground, J. Phys. Math. Nucl. Gen. 6 (1973) 1960.

[32] V.N. Bakatanov, A.E. Chudakov, A.E. Danshin, N.F. Klimenko, Yu.F. Novosel'tsev, Yu.V. Sten'kin, Stopping muons at the depth 850 hg/cm^2 underground, in: Proc. 16th ICRC, Kyoto, vol. 10, 1979, p. 175.

[33] S. Charalambus, Nuclear transmutation by negative stopped muons and the activity induced by the cosmic-ray muons, Nucl. Phys. A 166 (1971) 145–161.

[34] T. von Egidy, F.J. Hartmann, Average muonic Coulomb capture probabilities for 65 elements, Phys. Rev. A 26 (1982) 2355–2360.

[35] T. Suzuki, D.F. Measday, J.P. Roalsvig, Total nuclear capture rates for negative muons, Phys. Rev. C 35 (1987) 2212–2224.

[36] D. Lal, Annu. Rev. Earth Planet. Sci. 16 (1988) 355–388.

[37] K. Nishiizumi, E.L. Winterer, C.P. Kohl, J. Klein, R. Middleton, D. Lal, J.R. Arnold, Cosmic ray production rates of ^{10}Be and ^{26}Al in quartz from glacially polished rocks, J. Geophys. Res. 94 (1989) 17907–17915.

[38] K. Nishiizumi, R.C. Finkel, J. Klein, C.P. Kohl, Cosmogenic production of ^{7}Be and ^{10}Be in water targets, J. Geophys. Res. 101 (1991) 22225–22230.

[39] A.J.T. Jull, N. Lifton, W.M. Phillips, J. Quade, Studies of the production rate of cosmic-ray produced ^{14}C in rock surfaces, Nucl. Instrum. Methods B 92 (1994) 308–310.

[40] F.M. Phillips, M.G. Zreda, M.R. Flinsch, D. Elmore, P. Sharma, A reevaluation of cosmogenic ^{36}Cl production rates in terrestrial rocks, Geophys. Res. Lett. 23 (1996) 949–952.

[41] J.M. Evans, J.O.H. Stone, L.K. Fifield, R.G. Cresswell, Cosmogenic chlorine-36 production in K-feldspar, Nucl. Instrum. Methods B 123 (1997) 334–340.

[42] B. Heisinger, Determination of erosion rates with the cosmic-ray produced radioisotopes ^{26}Al and ^{53}Mn (in German), Diploma thesis, Technical University of Munich, Germany, 1994.

[43] K. Knie, Technical University of Munich, private communication, 1998.

[44] D. Lal, Cosmic ray labeling of erosion surfaces; in-situ production rates and erosion models, Earth Planet. Sci. Lett. 104 (1991) 424–439.

[45] M. Boezio et al., Measurement of the flux of atmospheric muons with the CAPRICE94 apparatus, Phys. Rev. D 62 (2000) 032007.

[46] D.C. Rose, K.B. Fenton, J. Katzman, J.A. Simpson, Latitude effect of the cosmic ray nucleon and meson components at sea level from the Arctic to the Antarctic, Can. J. Phys. 34 (1956) 968–984.

[47] R.C. Reedy, K. Nishiizumi, J. Klein, R. Davis, R. Middleton, D. Lal, J.R. Arnold, P. Kubik, A.J.T. Jull, P.A.J. Englert, D. Elmore, Production of cosmogenic-nuclides by muons, Abstract 8th Int. Conf. Geochronology, Cosmochronology and Isotope Geology, U.S. Geological Survey Circular 1107 (1994) 262.

[48] K.J. Kim, P.A. Englert, R. Finkel, D. Krofcheck, Cosmic-ray induced ^{10}Be and ^{26}Al in subsurface samples from Macraes Flat, East Otago, New Zealand, EOS Trans. Am. Geophys. Union 80 (1999) F1166–F1167.

[49] E.T. Brown, D.L. Bourles, F. Colin, G.M. Raisbeck, F. Yiou, S. Desgarceaux, Evidence for muon-induced production of ^{10}Be in near-surface rocks from the Congo, Geophys. Res. Lett. 22 (1995) 703–706.

[50] D. Lal, B. Peters, Cosmic ray produced radioactivity on the Earth, in: Handbuch der Physik 46, 2, Springer, Berlin, 1967, pp. 551–612.

[51] P. Goldhagen, M. Regginatto, T. Kniss, J.W. Wilson, R.C. Singleterry, I.W. Jones, W. Van Steveninck, Measurement of the energy spectrum of cosmic-ray induced neutrons aboard an ER-2 high-altitude airplane, Nucl. Instum. Methods A 476 (2002) 42–51.